THE JOURNAL OF PHYSICAL CHEMISTRY A

 VOLUME 113, NUMBER 50, DECEMBER 17, 2009

FEATURE ARTICLE

Optimization of Exciton Trapping in Energy Transfer Processes

Jianshu Cao* and Robert J. Silbey*

Department of Chemistry, Massachusetts Institute of Technology, Cambridge, Massachusetts 02139

Received: April 8, 2009; Revised Manuscript Received: October 2, 2009

In this paper, we establish optimal conditions for maximal energy transfer efficiency using solutions for multilevel systems and interpret these analytical solutions with more intuitive kinetic networks resulting from a systematic mapping procedure. The mapping procedure defines an effective hopping rate as the leading order picture and nonlocal kinetic couplings as the quantum correction, hence leading to a rigorous separation of thermal hopping and coherent transfer useful for visualizing pathway connectivity and interference in quantum networks. As a result of these calculations, the dissipative effects of the surrounding environments can be optimized to yield the maximal efficiency, and modulation of the efficiency can be achieved using the cumulative quantum phase along any closed loops. The optimal coupling of the system and its environments is interpreted with the generic mechanisms: (i) balancing localized trapping and delocalized coherence, (ii) reducing the effective detuning via homogeneous line-broadening, (iii) suppressing the destructive interference in nonlinear network configurations, and (iv) controlling phase modulation in closed loop configurations. Though these results are obtained for simple model systems, the physics thus derived provides insights into the working of light harvesting systems, and the approaches thus developed apply to large-scale computation.

I. Introduction

In photosynthetic systems, excitation energy is transferred between pigments of the antenna to reach the reaction centers with remarkable efficiency.[1−3] Recent experiments reveal that photosynthetic systems and their surrounding protein environments interact coherently to optimize transfer pathways and maximize efficiency.[4,5] The high efficiency in natural systems has inspired scientists to design artificial systems for efficient conversion of solar energy into useful energy forms.[6] These experimental results have motivated two theoretical questions: how to optimize the efficiency of energy transfer systems in dissipative environments and how to understand the optimization conditions in terms of classical kinetics. In the following, we elaborate on these two questions and outline the approaches to address them, then review related papers published recently, and finally establish the connection between quantum control theory and optimal design theory.

A. Motivations and Outline. In an energy transfer process characterized by quantum coherence, trapping, and dissipation,[7−14] how can one optimize the interplay of different mechanisms to achieve the best quantum efficiency under certain physical constraints? Naively, one would think that a one-dimensional linear configuration with no dissipation would be ideal. However, such a system is highly coherent and delocalized in space and does not trap easily into the target state, thus resulting in low quantum yield for energy conversion.[15−17] In section III, we discuss the optimization conditions of coherence, trapping, and dissipation for maximal quantum efficiency of energy transfer systems in linear configurations. For nonlinear configurations with spatial arrangements, quantum effects become

10.1021/jp9032589
Published on Web 11/24/2009

more dramatic due to the interference between different pathways, giving rise to the phase modulation of the efficiency.[18] The added complexity of reversible transitions, dephasing, and detuning makes the prediction of phase modulation more subtle in photosynthetic pigments, dendrimers, molecular wires, polymeric liquid crystals, and other quantum transport systems with nonlinear spatial configurations. Phase modulation plays an interesting role in laser experiments, where relative phases between different matrix elements and between different excitation pathways can be introduced and controlled.[19−22] In section V we study the phase modulation in multisite systems and extend the conclusions to general scenarios of nonlinear molecular arrangements.

Much of our discussion is based on exact analytical solutions for model systems. Though the same physics is expected, exact solutions for large photosynthetic systems and other realistic systems become impractical if not impossible. How can we develop an intuitive understanding of the underlying physics in a complex system and systematically predict quantum effects? Often, energy transfer in photosynthetic systems is pictured as a stepwise hopping process, where adjacent sites are linked with a hopping rate. In section IV, we map an energy transfer network to a kinetic network as the leading order picture and use it as the basis to formulate a systematic expansion of the full quantum mechanical treatment. The expansion assigns nonlocal links between states, which is a manifestation of quantum coherence and delocalization. The mapping to kinetic networks takes advantage of perspectives such as modularity, pathway decomposition, and flux balance, provides a kinetic picture of quantum dynamic effects including coherence, delocalization, and interference, and introduces a starting point for further discussions on robustness of energy transfer networks.

The rest of paper is organized as follows: In section II, we define the model system, energy transfer efficiency (i.e., quantum yield), and its relationship to the average trapping time in the high-yield limit. In section III, we establish the optimization conditions for maximal efficiency or minimal trapping time in one-dimensional multisite chain systems. In section V, we formulate the systematic procedure to map energy transfer networks to kinetic networks with both local and nonlocal links. In section V, we predict the phase modulation of efficiency for energy transfer systems with topological loop(s) using analytical solutions, numerical calculations, and the kinetic mapping approach. In section VI, we conclude the paper by summarizing our findings.

B. Survey of Related Studies. The exactly solvable models studied here not only quantify the key results in the literature but also suggest new observations that have not been predicted. Here, we discuss the implications of our results in the context of recent publications.

1. Energy transport in molecular crystals and aggregates has been extensively reviewed, usually focusing on the diffusive limit of extended systems.[15] Interestingly, the exciton diffusion constant on an infinite lattice is shown to reach a maximal value at an optimal dephasing rate, a result relevant for quantum transport in nanoscale systems. However, in the presence of the trapping at the charge transfer state, energy transfer is biased toward the trap state and, different from random walk in an infinite lattice, exciton transfer and trapping may not necessarily occur in the diffusive limit.
2. Early calculations of energy transfer in molecular aggregates are based on classical kinetics with rates estimated by Forster theory and Dexter theory. This approach is equivalent to the first order of the kinetic mapping procedure introduced in section IV and is applicable to energy transfer systems without strong coherent effects. In a series of studies, Sener and Schulten demonstrated the robustness of photosynthetic networks by examining variations in energy transfer efficiency in response to changes in rate constants, temperatures, and connectivity.[11,12] Knoester and co-workers discussed dendrimes and cylindrical aggregates and explored the relationship between network connectivity and trapping time within the framework of classical kinetics.[23,24]
3. Quantum mechanical effects in finite exciton systems can be explicitly included by using the density matrix and quantum master equations. The quantum treatment is essential for calculating spectral properties for molecular aggregates and has also been extended to transport properties. For example, Reineker et al. calculated optical absorption and energy transfer in dendrimers, and showed

Jianshu Cao is an associate professor of chemistry at MIT. He received a Ph.D. in physics from Columbia University in 1993, under the direction of Bruce Berne. After postdoctoral research with Greg Voth at University of Pennsylvania and with the late Kent Wilson at UCSD, he jointed the MIT faculty in 1998. His research interests include quantum dynamics of molecular systems, stochastic analysis of single molecule measurements, self-assembly of colloids and polymers, and mechanical properties of cells and bio-molecules.

Bob Silbey received his Ph.D. at the University of Chicago working with Professor Stuart Rice, after which he worked as an AFOSR postdoctoral fellow with Professor Joseph Hirschfelder at the University of Wisconsin. He has spent his entire academic career as a faculty member at MIT, except for visiting professorships in The Netherlands, France, and Germany. Silbey has done research on energy and electron transfer in condensed phases, energy transfer from excited molecules to surfaces, electronic states and optical properties of conjugated polymers, quantum dynamics of tunneling systems interacting with their environment, the coupling of vibrational and electronic degrees of freedom in molecules and solids, and the quantum dynamics of highly excited molecules. He has worked very closely with experimentalists in all his research.

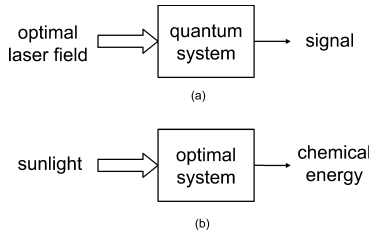

Figure 1. Schematic illustration of (a) quantum control theory and (b) optimal design theory.

the time-dependence of energy transport and the dominance of the rim states in the absorption spectra.[25,26] Other quantum calculations include impurity quenching of Frenkel excitons in linear chains[27] and nonmonotonic dependence of energy harvesting efficiency in biased exciton chains.[28]

4. Inspired by time-resolved spectroscopy measurements, several groups explored the optimization conditions of exciton transfer and trapping. Of particular relevance are the numerical solutions by Gaab and Bardeen for N-site homogeneous chain systems in different topological arrangements. They predicted the optimal combination of trapping and dephasing for the minimal trapping time.[29] Recent studies by Plenio and co-workers on linear chain models and on globally connected network models show explicitly the dependence of transfer efficiency on energy mismatch (i.e., detuning) and dephasing rate.[30,31] Optimal conditions have also been identified for a local site model of the FMO complex.[32−34] A recent quantum calculation of LH2 demonstrates the role of quantum coherence in disordered biological systems and the importance of the initial preparation of quantum states.[35]

Our solutions of multilevel systems not only quantify the results reported in the above studies but also make new predictions, including the lack of environment-assistance in linear-chain systems and the phase-dependence in a close network. The analysis of the two-level and three-level models allows us to understand and classify the optimal conditions of complicated model systems in a simple and unified framework.

C. Quantum Control and Optimal Design. The optimization analysis reported here is related to another important development in physical chemistry, i.e., the application of optimal control theory to coherent excitation of chemical systems. Stimulated by advances of ultrafast laser technology, quantum control theory addresses the question of how to design an optimal laser field to drive the dynamics of a quantum system for selective chemical bond formation and breaking.[36−40]

1. For photosynthetic systems, the inputs are incoherent photons from sunlight and are a given constraint under specific ambient conditions. Instead of optimizing laser fields, we optimize the design of photosynthetic systems for energy transfer and subsequent conversion to chemical energy. Specifically, coherent control theory searches for the best laser field given the system Hamiltonian,[41] whereas optimal design theory searches for the best system Hamiltonian given the input photons. Though different in their formulations, both theories as illustrated in Figure 1 aim to optimize the efficiency of photons to achieve an objective.
2. In the Gaussian bath representation, the stochastic force exerted by the environment $f(t)$ is analogous to the laser field $E(t)$, which is harmonic in second quantization. Thus, the search for the optimal dephasing mechanism is similar to the search for the driving force to guide the system along a specific trajectory, although the environment often consists of a continuous distribution of modes and the electric field can be a single mode. In a sense, optimization of exciton trapping can be regarded as an application of optimal control theory to a new class of problems related to the design of molecular structures. Broadly speaking, optimal design theory not only explores the structure−function relation for the best design of efficient artificial photosynthetic systems but also helps to explore the implications of evolution and environmental selection in natural photosynthetic systems.[42]
3. In addition, the energy transfer and trapping problem also poses an interesting quantum coherent control problem. In the multiple site solutions, the transfer efficiency depends on the initial population or more generally on the initial density matrix; thus, one can design the laser field to prepare the optimal initial state of the exciton system to achieve the best transfer efficiency. In fact, a recent paper demonstrates the crucial role of the quantum superposition of the initial state in the energy transfer process of the LH1-RC core unit and suggests a case study of optimal excitation in light-harvesting systems.[35]

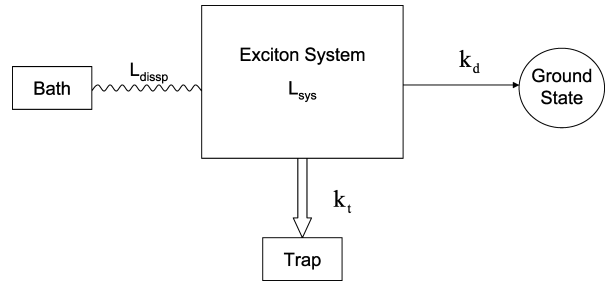

Figure 2. Schematic illustration of the exciton system coupled to the dissipative environment and subject to decay to the ground state and trapping at the charge transfer state.

II. Quantum Efficiency and Average Trapping Time

To formulate the problem, we begin with the equation of motion for the exciton system depicted in Figure 2,

$$\dot{\rho}(t) = -\mathscr{L}\rho(t) = -[\mathscr{L}_{sys} + \mathscr{L}_{dissip} + \mathscr{L}_{decay} + \mathscr{L}_{trap}]\rho(t) \quad (1)$$

where ρ is the density matrix. In eq 1, $\mathscr{L}_{sys}$ is the evolution operator of the isolated exciton system. An isolated quantum system is completely coherent and exhibits oscillatory behavior that does not yield net energy flux. The mechanisms responsible for irreversible energy flow include the coupling to the solvent environment, the finite exciton lifetime, and the trapping at the charge separation state for subsequent conversion to chemical energy. $\mathscr{L}_{dissip}$ represents the dephasing and population effects within the exciton manifold. $\mathscr{L}_{decay}$ represents the decay of the exciton to the ground state to produce heat and can be expressed as $[\mathscr{L}_{decay}]_{nm} = ([k_d]_n + [k_d]_m)/2$ with k_d the decay rate. $\mathscr{L}_{trap}$ represents the trapping of the exciton at the charge separation state and can be expressed as $[\mathscr{L}_{trap}]_{nm} = ([k_t]_n + [k_t]_m)/2$ with k_t the trapping rate. The system operator $\mathscr{L}_{sys}$ and the dissipation operator $\mathscr{L}_{dissip}$ depend on the details of the system−bath Hamiltonian. Specifically, we write $\mathscr{L}_{sys}\rho = i[H, \rho]/\hbar$, where $[H]_{nm} = (1 - \delta_{nm})J_{nm} + \delta_{nm}\epsilon_n$ with J_{nm} the next neighbor

coupling constant and ϵ the site energy. When the coupling matrix element J_{nm} carries a phase, the complex coupling matrix must be Hermitian, $J_{nm} = J_{mn}^*$. As mentioned earlier,[19−21] in optical experiments, the relative phase between different coupling matrix elements associated with distinct excitation pathways can be controlled by coherent laser fields. For the convenience of analysis, the coupling to the environment is described by the standard Bloch−Redfield equation, $[\mathscr{L}_{\text{dissip}}]_{nm} = (1 - \delta_{nm})\Gamma_{nm}^*$, with Γ^* the pure dephasing rate. More complicated forms of quantum master equations[43−45] can be incorporated in the future but will not be discussed here. In this paper, we consider only the dephasing and ignore population relaxation between different states within the exciton manifold.

We first comment on the model system defined in Figure 2 and in eq 1. (i) The full exciton−bath Hamiltonian includes both the dynamic relaxation to the ground state and the dynamic localization (i.e., trapping) at the charge transfer state. In our model, both mechanisms are represented by kinetic rate constants, k_{d} and k_{t}, respectively. This simplification can be justified by time-scale separation and can be removed in a full-scale quantum dynamic simulation. (ii) Often, dynamic noise appears in both the diagonal and off-diagonal matrix elements of the system Hamiltonian, leading to two different relaxation channels. It is believed that the diagonal disorder is dominant in photosynthetic systems and dephasing is the primary relaxation mechanism. (iii) The master equation formulation depends on the choice of the basis set, to which the Markovian approach is applied. The choice of the basis set depends on the strength of system−bath coupling and on the measurement time scale. Except for systems of high symmetry, such as LH2, energy transfer is usually described in the local basis set, classically as hopping or quantum mechanically using quantum master equations. On the basis of the physical considerations, we adopt the local basis set and assume the high-temperature limit. Combining these approximations, we arrive at eq 1, where the system dynamics with the approximation in eq 3 (without explicit consideration of exciton decay) is the same as the Haken−Strobl model.

According to eq 1, $\mathscr{L}_{\text{decay}}$ and $\mathscr{L}_{\text{trap}}$ represent two possible channels for irreversible exciton energy loss, one ineffective energy transfer, and the other effective. Then the efficiency of energy transfer is gauged by the quantum trapping yield, q, defined as the trapping probability[46]

$$q = \frac{\sum_n k_{\text{t},n}\tau_n}{\sum_n k_{\text{t},n}\tau_n + \sum_n k_{\text{d},n}\tau_n} \tag{2}$$

Here, τ_n is the mean residence time defined as the integral over the population, i.e., $\tau_n = \int_0^\infty \rho_n(t)\,\mathrm{d}t$, and the population $\rho_n = \rho_{n,n}$ is the diagonal element of the density matrix. The denominator in eq 2 is the total depletion probability, which for convenience is normalized to unity. It then follows that $(1 - q)$ represents the probability of exciton energy dissipation to heat during transfer processes and can be minimized by reducing the residence time the system spends on the transfer pathway. Without loss of generality, we consider constant exciton decay rate k_{d} and trapping localized at the terminal state (charge transfer state) k_{t}. When the quantum yield is close to unity, the trapping rate is much larger than decay rate, i.e., $k_{\text{d}}/k_{\text{t}} \ll 1$, so that we can ignore the k_{d} dependence in the mean residence time, $\tau(k_{\text{d}}) \approx \tau(0)$, and thus $\Sigma k_{tn}\tau_n(k_{\text{d}}) = 1$. Then, the quantum yield can be approximated as

$$q \approx \frac{1}{1 + \sum_n k_{\text{d},n}\tau_n(k_{\text{d}} = 0)} = \frac{1}{1 + k_{\text{d}}\langle t\rangle} \tag{3}$$

where $\langle t\rangle$ is the mean first passage time to the trap state without the presence of the constant decay, i.e., the average trapping time, and is expressed in terms of the mean residence time as $\langle t\rangle = \Sigma_n\tau_n$ and we assume k_{d} is the same for all sites. Since only the average trapping time $\langle t\rangle$ is needed in eq 3, we invoke the stationary solution to eq 1, $\mathscr{L}\tau = \rho(0)$ or $\tau = \mathscr{L}^{-1}\rho(0)$, such that the average trapping time is given by $\langle t\rangle = \Sigma_n\tau_n = \Sigma_{nm}\mathscr{L}_{nm}^{-1}\rho_m(0)$. In this paper, we set the initial distribution $\rho(0)$ to be localized at the donor state, $\rho_n(0) = \delta_{n,1}$ and $\rho_{nm} = 0$, and set the trapping rate to $k_{t,n} = k_t\delta_{n,N}$ with N denoting the terminal state. Equation 3 allows us to estimate the parameter range where the transfer efficiency remains approximately constant.[34]

Quantum yield and trapping time have been extensively studied in the context of single molecule photon statistics.[46] In fact, single molecule spectroscopic experiments have been carried out on photosynthetic systems to demonstrate the broad distribution in their photophysical properties.[3,47] With the single molecule technique, it is now possible to measure not only the mean first passage time but also its distribution. The calculation of such distributions and their physical implications will be a subject of interest for further studies.

III. Linear Configuration: Optimal Environments

Recent experiments suggest that photosynthetic systems and surrounding protein environments interact coherently to achieve the most efficient exciton energy transfer.[4,5] Motivated by the experimental findings, we derive analytical solutions for the two-site, three-site, and N-site chain systems and identify optimal conditions of dissipative environments for minimal trapping time. These model studies can be extended to analyze exciton energy transfer in photosynthetic systems and to characterize the optimization conditions for maximal quantum yield. The simple analytical solutions derived here may not be available for realistic systems, but the basic physics will remain the same.[34]

A. Two-Site System. As the first example, we consider a two-site system, or equivalently, the standard quantum two-level system (TLS). For this simple problem, the average trapping time can be easily calculated to give

$$\langle \text{t}\rangle = \frac{2}{k_t} + \frac{1}{2J^2}\frac{\Gamma^2 + \Delta^2}{\Gamma} \tag{4}$$

where $J = J_{12}$ is the off-diagonal coupling constant, $\Delta = \epsilon_2 - \epsilon_1$ is the detuning, and $\Gamma = \Gamma^* + k_t/2$ is the phase relaxation rate for the off-diagonal matrix element. Equation 4 has appeared in standard references and more recently in the context of single molecule spectroscopy. Examination of eq 4 suggests the existence of the minimal trapping time, i.e., maximal quantum yield, for a given set of J and Δ:

- With a fixed pure dephasing rate, there is an optimal trapping rate as a function of Γ^* in the range of $2(2^{1/2})J < k_{\text{t}} < 2(2J^2 + \Delta^2)^{1/2}$. The upper limit is obtained by setting $\Gamma^* = 0$ and the lower limit is obtained by taking larger value of Γ^*.
- With a fixed trapping rate, if $k_{\text{t}} < 2\Delta$, the optimal dephasing rate is $\Gamma^* = \Delta - k_t/2$ and the minimal trapping time is $\langle t\rangle = 2/k_{\text{t}} + \Delta/J^2$. If $k_{\text{t}} > 2\Delta$, the optimal dephasing rate is Γ^*

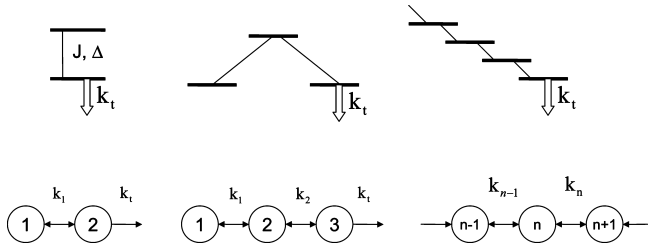

Figure 3. Schematic representations of the two-site system, three-site system, and *N*-site system, with corresponding kinetic schemes in the leading order.

$= 0$ and the minimal trapping time is $\langle t\rangle = (2J^2 + \Delta^2)/(k_t J^2) + k_t/(4J^2)$.

- The general optimal condition is $\Gamma^* = 0$ and $k_t = 2(2J^2 + \Delta^2)^{1/2}$. The minimal trapping time is $\langle t\rangle = (2J^2 + \Delta^2)^{1/2}/(2J^2)$.

To confirm the optimal conditions derived above, we plot the average trapping time as a function of trapping rate k_t and dephasing rate Γ^* in Figure 4. For the on-resonant case ($\Delta = 0$), there is always a nonzero value for the optimal trapping rate but a zero value for the optimal dephasing rate. For the off-resonant case ($\Delta = 3J$), with a given trapping rate k_t, the optimal dephasing rate is nonzero for $k_t < 2\Delta$, and zero for $k_t > 2\Delta$.

These optimal conditions can be understood with simple physical arguments. For example, while fast trapping at state 2 obviously enhances energy transfer, the fast population relaxation at state 2 also destroys the phase coherence between states 1 and 2 and therefore reduces the effective population transfer rate between the two states, i.e., k_1 in eq 10. Hence, there exists an optimal trapping rate that minimizes the average energy transfer time. Also, in the presence of large energy difference Δ and slow trapping rate ($k_t < 2\Delta$), efficient energy transfer is achieved when the broadened line width due to dephasing overlaps with the detuning, thus suggesting an optimal pure dephasing rate.

Before turning to the next example, we explicitly evaluate the quantum yield in eq 2 and confirm the slow decay approximation adopted in eq 3. We can use the standard solution to the two-site system with the depletion rate $k_1 = k_d$ and $k_2 = k_d + k_t$ and the dephasing rate $\Gamma = \Gamma^* + k_t/2 + k_d$. Then, the quantum yield in eq 2 reads

$$\begin{aligned} q &= k_t\tau_2(k_d) = \frac{k_t}{k_2}\frac{2J^2}{2J^2\left(1+\frac{k_1}{k_2}\right)+k_1\left(\Gamma+\frac{\Delta^2}{\Gamma}\right)} \\ &= \frac{k_t}{k_t + 2k_d + \frac{k_d}{2J^2}(k_d+k_t)\left(\Gamma+\frac{\Delta^2}{\Gamma}\right)} \approx \\ &\quad \frac{1}{1+k_d\langle t\rangle} + O\left(\frac{k_d^2\langle t\rangle}{k_t}\right) \end{aligned} \tag{5}$$

where the second line is rearranged for easy comparison with eq 4. Evidently, in the limit of $k_d/k_t \ll 1$, the k_d dependence in Γ and the last term in the denominator can be ignored, such that we recover the simpler expression in eq 3. As expected, the leading order correction in eq 5 is on the order of k_d/k_t. For the remaining part of the paper, we will focus on the calculation of the average trapping time and assume that quantum yield is given by eq 3 in the limit of small decay rate or high quantum yield.

B. Three-Site System in the Linear Configuration. Our second example of energy transfer along a linear chain is the three-site system, with a donor, an acceptor, and a bridge state, as shown in Figure 3. We consider the symmetric case where $\epsilon_1 = \epsilon_3$. With the approach outlined above, we obtain

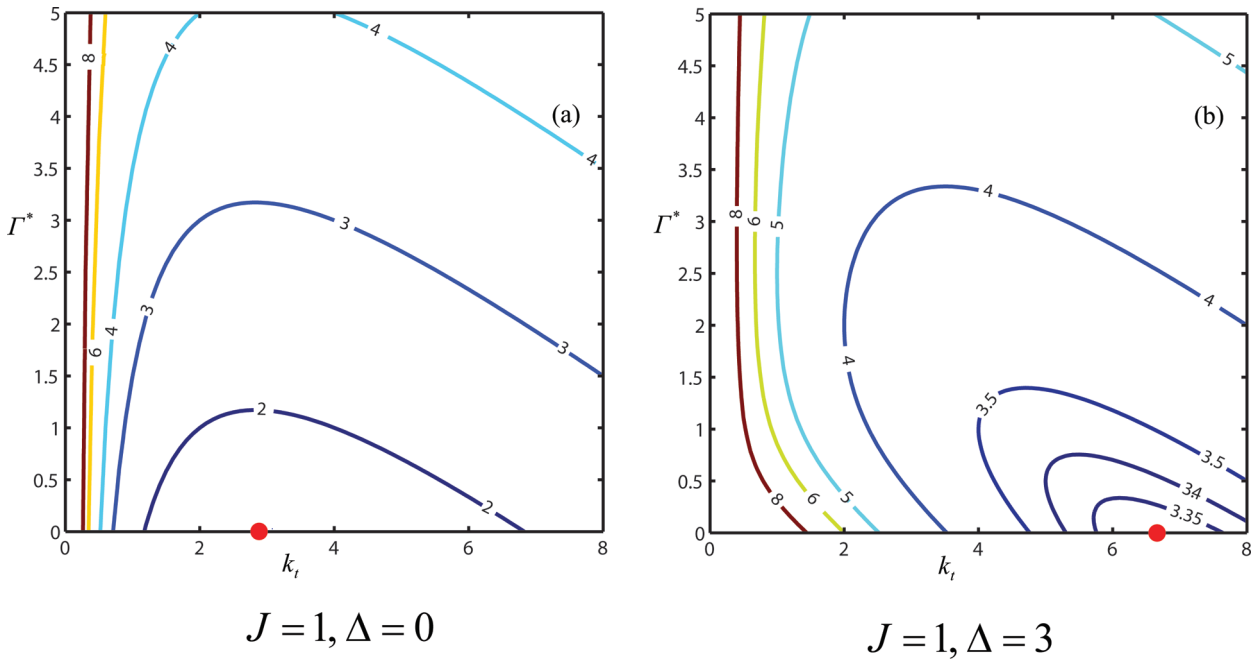

Figure 4. Average trapping time as a function of trapping rate k_t and dephasing rate Γ^* for the two-level system (a) with $|J| = 1$ and $\Delta = 0$ (the left contour plot) and (b) with $|J| = 1$ and $\Delta = 3$ (the right contour plot). The solid circle represents the global minimal.

$$\begin{aligned}\langle t\rangle &= \frac{3}{k_t}+\frac{2}{k_2}+\frac{1}{k_1}\\ &= \frac{3}{k_t}+\frac{1}{|J_{23}|^2}\left[\Gamma_{23}-\frac{1}{\Gamma_{31}}(|J_{23}|^2-|J_{12}|^2)+\frac{\Delta^2}{\mathrm{Det}}\Gamma_{12}\right]+\\ &\quad \frac{1}{2|J_{12}|^2}\left[\Gamma_{12}+\frac{1}{\Gamma_{31}}(|J_{23}|^2-|J_{12}|^2)+\frac{\Delta^2}{\mathrm{Det}}\Gamma_{23}\right]\end{aligned} \tag{6}$$

where $\Delta_{12}=-\Delta_{23}=\Delta$, $\Delta_{31}=0$, $\Gamma_{12}=\Gamma_{12}^*$, $\Gamma_{23}=\Gamma_{23}^*+k_t/2$, $\Gamma_{31}=\Gamma_{31}^*+k_t/2$, and $\mathrm{Det}=\Gamma_{12}\Gamma_{23}+(|J_{23}|^2\Gamma_{23}+|J_{12}|^2\Gamma_{12})/\Gamma_{31}$. Under the special condition of identical coupling constants $J=J_{12}=J_{23}$ and identical dephasing rates $\Gamma^*=\Gamma_{12}^*=\Gamma_{23}^*=\Gamma_{31}^*$, eq 6 reduces to

$$\langle t\rangle = \frac{3}{k_t}+\frac{1}{2J^2}\left[(k_t+3\Gamma^*)+\Delta^2\frac{k_t/2+3\Gamma^*}{(k_t/2+\Gamma^*)\Gamma^*+J^2(k_t+4\Gamma^*)/(k_t+2\Gamma^*)}\right] \tag{7}$$

Careful examination of eq 7 establishes the optimal conditions for the near-resonant case as $\Gamma^*=0$ and $k_t=[3(\Delta^2+2J^2)]^{1/2}$ and the optimal trapping time as $\langle t\rangle = 1/(J^2+\Delta^2/2)^{1/2}$. We will see in section IV that a three-site system can be mapped to a system of three kinetic states so that the three terms in eq 6 follow the general functional form for a kinetic chain reaction (see eq 15 below).

To examine the optimal conditions, we plot the average trapping time as a function of trapping rate k_t and dephasing rate Γ^* in Figure 5. Similar to the two-level system, the near-resonant case ($\Delta=0.1J$), the optimal trapping time is obtained without dephasing but with a finite trapping rate. Different from the two-level system, for the far-off resonant case ($\Delta=3J$), the optimal trapping time is obtained with nonvanishing dephasing rate and trapping rate.

C. *N*-Site Chain System. Our last example is an *N*-site system in the linear configuration. The general solution of the *N*-site linear chain system is difficult to obtain if not impossible. Instead, we adopt the more intuitive approach of mapping a quantum exciton system to a classical kinetic network. The mapping is explicitly formulated in section IV, where the classical rate expressions (see eqs 14 and 15) give

$$\langle t\rangle \approx \frac{N}{k_t}+\frac{1}{2}\sum_{n=1}^{N-1}\left[\Gamma_{n,n+1}+\frac{\Delta_{n,n+1}^2}{\Gamma_{n,n+1}}\right]|J_{n,n+1}|^2 \tag{8}$$

Consider the special case of constant detuning Δ, constant coupling constant J, and constant dephasing rate Γ^*. Then, eq 8 reduces to

$$\langle t\rangle = \frac{N}{k_t}+\frac{N-1}{2J^2}\left[\frac{N\Gamma^*}{2}+\frac{k_t}{2}+\frac{\Delta^2}{\Gamma^*+k_t/2}\right] \tag{9}$$

which leads to the following observations:

- With a fixed trapping rate, the optimal dephasing rate is $\Gamma^*=(2/N)^{1/2}\Delta-k_t/2$, if $k_t<2(2/N)^{1/2}\Delta$ and is zero, $\Gamma^*=0$, if $k_t>2(2/N)^{1/2}\Delta$.
- The general optimal condition is $\Gamma^*=0$ and $k_t=2[\Delta^2+NJ^2/(N-1)]^{1/2}$, and the minimal trapping time is $\langle t\rangle=(N-1)[\Delta^2+NJ^2/(N-1)]^{1/2}/J^2$, for a given set of J and Δ.

Evidently, the optimal conditions discussed for the two-site system is a special case of the above observations with $N=2$. Also note that for a long chain the optimal trapping time increases linearly with N, $\langle t\rangle = N(\Delta^2+J^2)^{1/2}/J^2\propto N$, confirming the linear scaling of extended dissipative exciton systems. Numerical calculations of the *N*-site Bloch equation indicates the accuracy of the approximate classical solution in eq 8 improves with the number of the sites, thus suggesting the validity of mapping of an extended exciton system to a kinetic network.

IV. Mapping to Kinetic Networks

The energy transfer units in photosynthetic systems exhibit rich topological connectivity that facilitates fast and robust energy harvesting. The topological connectivity in such complex molecular architectures is often analyzed using the language of kinetic networks, as for chemical networks or electric circuits. However, excitons are quantum mechanical states that cannot be readily represented by classical kinetic states. In fact, for isolated exciton systems described by $\mathscr{L}_{\mathrm{sys}}$, all local sites are entangled and coherence extends over the whole space. Fortunately, in realistic photosynthetic systems, various dissipative mechanisms and decay channels act together to truncate the spatial-temporal range of quantum coherence and to introduce a local nature to exciton states. As a result, we can map the structure of exciton systems to networks and thus develop an intuitive understanding of the spatial arrangements and their role in the optimization of exciton transfer efficiency.[34]

A. Classical Kinetic Rate. To demonstrate this approach, we examine exciton transfer in linear chains. Our first example is the simple two-site system described in Figure 3. The stationary condition on the off-diagonal density matrix element ρ_{12} leads to $\rho_{12}\approx \mathrm{i}J(\rho_1-\rho_2)/(\Gamma+\mathrm{i}\Delta)$. Inserting this expression into the equation of motion for the two diagonal matrix elements, we arrive at $\dot\rho_1=-k_1(\rho_1-\rho_2)$ and $\dot\rho_2=k_1(\rho_1-\rho_2)-k_t\rho_2$, where $k_1=2\Gamma J^2/(\Gamma^2+\Delta^2)$ is the effective rate constant between the two states. As a result, the two quantum levels reduce to the two kinetic states in Figure 3 and we can easily arrive at the average trapping time

$$\langle t\rangle = \frac{2}{k_t}+\frac{1}{k_1} \tag{10}$$

which recovers the result in eq 4. The same approach can be extended to three-state systems, four-state systems, or *N*-state systems.

For a general *N*-state system in the linear chain configuration, the off-diagonal matrix element follows

$$\dot\rho_{n,n+1}=\mathrm{i}(\rho_n J_{n,n-1}-J_{n,n+1}\rho_{n+1})+\mathrm{i}(\rho_{n,n+2}J_{n+2,n+1}-J_{n,n-1}\rho_{n-1,n+1})-\tilde\Gamma_{n,n+1}\rho_{n,n+1} \tag{11}$$

with $\Delta_{n,n+1}=\epsilon_n-\epsilon_{n+1}$ and $\tilde\Gamma_{n,n+1}=\Gamma_{n,n+1}+i\Delta_{n,n+1}$. On the right-hand-side of the equation, the first term represents the coupling between adjacent sites, and the second term represents the coupling beyond next adjacent sites. In a dissipative system, the effective coupling strength between sites decreases with separation; thus we can ignore nonadjacent site coupling in the leading order treatment and obtain under the stationary condition

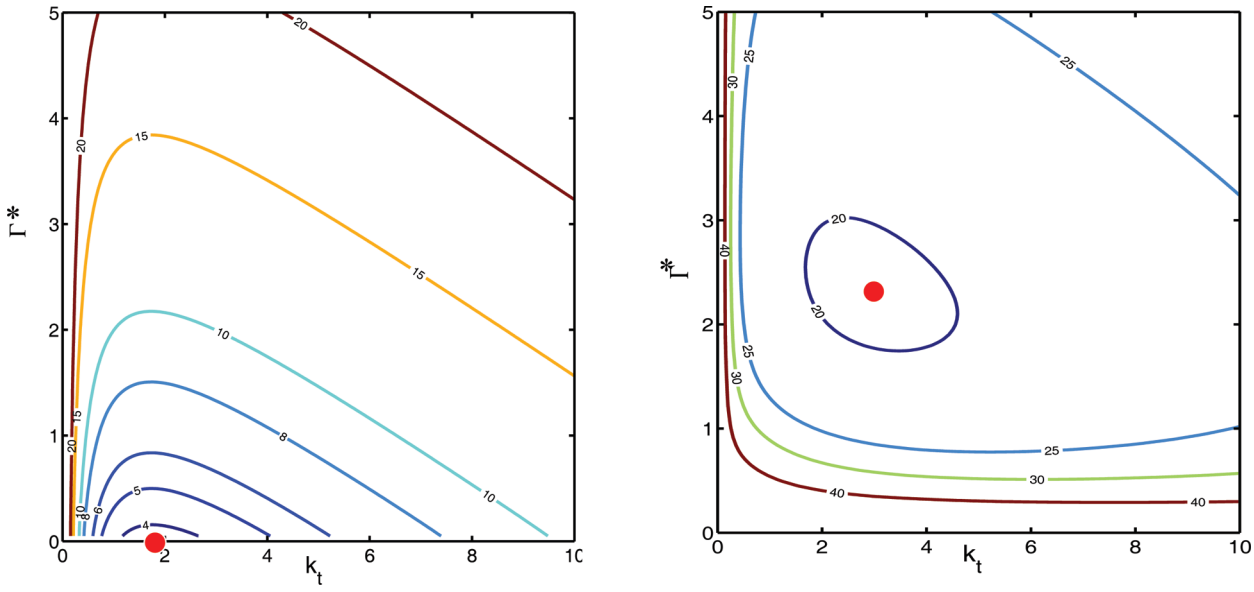

Figure 5. Average trapping time as a function of trapping rate k_t and dephasing rate Γ^* for the linear three-level system (a) with $|J| = J = 1$ and $\Delta = 0.1$ (the left contour plot) and (b) with $|J| = J = 1$ and $\Delta = 3$ (the right contour plot). The solid circle represents the global minimal.

$$\rho_{n,n+1} \approx \mathrm{i}\frac{J_{n,n+1}}{\tilde{\Gamma}_{n,n+1}}(\rho_n - \rho_{n+1}) \tag{12}$$

Inserting the stationary solution for the off-diagonal matrix element into the equation of motion for the diagonal matrix element, i.e.,

$$\dot{\rho}_n = (\mathrm{i}\rho_{n,n-1}J_{n-1,n} - \mathrm{i}J_{n,n-1}\rho_{n-1,n}) + (\mathrm{i}\rho_{n,n+1}J_{n+1,n} - \mathrm{i}J_{n,n+1}\rho_{n+1,n}) \tag{13}$$

we arrive at the rate equation, $\dot{\rho}_n = -k_{n,n+1}(\rho_n - \rho_{n+1}) + k_{n-1,n}(\rho_{n-1} - \rho_n) - \delta_{n,N}k_t\rho_n$, with effective rate constant

$$k_{n,n+1} = \frac{2\Gamma_{n,n+1}}{\Gamma_{n,n+1}^{\ 2} + \Delta_{n,n+1}^{\ 2}}|J_{n,n+1}|^2 \tag{14}$$

With this mapping, we can evaluate the average trapping time for the N-state linear chain and predict

$$\langle t \rangle = \frac{N}{k_t} + \cdots + \frac{2}{k_2} + \frac{1}{k_1} \tag{15}$$

which is a simple case of the chain reaction discussed recently (Appendix D of ref 46). Evidently, eqs 4 and 10 are a special case of the general expression with $N = 2$.

B. Quantum Corrections: Nonlocal Kinetics. To the leading order, the off-diagonal matrix element between two adjacent states simply provides an effective coupling and defines the rate constant for the population relaxation between the two states. In this sense, the leading order mapping constructs a kinetic network with effective local links and does not incorporate any nontrivial quantum coherent effects. To go beyond the leading order construction, we will have to include the nonadjacent terms in eq 11, which follow another equation of motion that couples to states further apart. A procedure can be established by systematically truncating the range of coupling in the equation for the off-diagonal matrix element. Let us take the example of the N-state chain system discussed earlier. Due to limited space, we will not include a detailed derivation but present the final result of the effective rate equation

$$\begin{aligned}\dot{\rho}_n = {} & k^+_{n-2,n-1}(\rho_{n-2} - \rho_{n-1}) + (k_{n-1,n} - k'_{n-1,n})(\rho_{n-1} - \rho_n) + k^-_{n,n+1}(\rho_n - \rho_{n+1}) - \\ & k^+_{n-1,n}(\rho_{n-1} - \rho_n) - (k_{n,n+1} - k'_{n,n+1}) \times (\rho_n - \rho_{n-1}) - k^-_{n+1,n+2}(\rho_{n+1} - \rho_{n+2})\end{aligned} \tag{16}$$

where k^+ and k^- are the feed-forward and feed-backward rate constants. With the leading order correction, the rate constants are given by

$$\begin{aligned} k'_{n,n+1} &= 2\mathrm{Re}\frac{|J_{n,n+1}|^2}{\tilde{\Gamma}_{n,n+1}^{\ 2}}\left(\frac{|J_{n-1,n}|^2}{\tilde{\Gamma}_{n-1,n+1}} + \frac{|J_{n+1,n+2}|^2}{\tilde{\Gamma}_{n,n+2}}\right) \\ k^+_{n-1,n} &= 2\mathrm{Re}\frac{|J_{n-1,n}|^2|J_{n,n+1}|^2}{\tilde{\Gamma}_{n-1,n}\tilde{\Gamma}_{n,n+1}\tilde{\Gamma}_{n-1,n+1}} \\ k^-_{n+1,n+2} &= 2\mathrm{Re}\frac{|J_{n,n+1}|^2|J_{n+1,n+2}|^2}{\tilde{\Gamma}_{n,n+1}\tilde{\Gamma}_{n+1,n+2}\tilde{\Gamma}_{n,n+2}} \end{aligned} \tag{17}$$

Comparison of eqs 14 and 17 suggests the small parameter in the approximate mapping as

$$\frac{|J_2|^2}{|\tilde{\Gamma}|^2} = \frac{|J|^2}{\Gamma^2 + \Delta^2} \ll 1 \tag{18}$$

which is satisfied under the condition of large dephasing rate rate $\Gamma > J$ or large detuning $\Delta > J$. In the example calculation,

we verify eq 18 by comparing the exact expression for the three-state system in eq 6 and the leading order expression in eq 14.

C. Example Calculations. To illustrate the mapping to classical kinetics, we study the three-site system described in section IIIB and in Figure 3. The rate constants defined in eq 13 become

$$\begin{aligned} k'_{12} &= 2\mathrm{Re}\frac{|J_{12}|^2|J_{23}|^2}{\tilde{\Gamma}_{12}{}^2\tilde{\Gamma}_{13}} \\ k'_{23} &= 2\mathrm{Re}\frac{|J_{12}|^2|J_{23}|^2}{\tilde{\Gamma}_{23}{}^2\tilde{\Gamma}_{13}} \\ k^{+}_{12} &= k^{-}_{23} = 2\mathrm{Re}\frac{|J_{12}|^2|J_{23}|^2}{\tilde{\Gamma}_{12}\tilde{\Gamma}_{23}\tilde{\Gamma}_{13}} \end{aligned} \tag{19}$$

where k' is the leading order correction for the local links and k^+ and k^- are the leading order corrections for the nonlocal links. The resulting rate matrix is $K = K_0 + K'$, with K_0 the classical rate and K' the leading order correction. The inverse matrix is expanded to leading order, giving $K^{-1} \approx K_0{}^{-1} - K_0{}^{-1}K'K_0{}^{-1}$. Then, we obtain the average trapping time

$$\langle t\rangle \approx \frac{3}{k_t} + \frac{2}{k_{23}}\left(1 - \frac{k^{+}_{12}}{k_{12}} - \frac{k'_{23}}{k_{23}}\right) + \frac{1}{k_{12}}\left(1 - \frac{k^{-}_{23}}{k_{23}} - \frac{k'_{12}}{k_{12}}\right) \tag{20}$$

where the second term is the effective $1/t_2$ and the third term is the effective $1/t_1$. For the special case of the symmetric three-site system analyzed in section IIIB, our results agree with the exact expression in eq 6 to leading order of J/Γ, thus confirming the accuracy of the mapping procedure.

D. General Procedure. In general, under the steady-state condition or in the case of fast dephasing, we can set the off-diagonal elements of the density matrix to the steady state and obtain a stationary condition that relates off-diagonal elements ρ_{OD} to diagonal matrix elements ρ_D. Then, the propagation of the diagonal matrix elements reduces to the rate equation

$$\dot{\rho}_D = \mathscr{L}_D\rho_D + \mathscr{L}_{OD}\rho_{OD} = -K\rho_D \tag{21}$$

where ρ_{OD} is expressed linearly in terms of ρ_D as $\rho_{OD} = M\rho_D$, and the rate matrix is defined as $K = -\mathscr{L}_D - \mathscr{L}_{OD}M$. Unlike a typical rate equation, eq 21 describes a complex rate process with feed-back and feed-forward, where the rate constant between a pair of states depends not only on their populations but also on the populations of a distant pair of states. This nonlocality reflects the delocalized nature of exciton states and is truncated due to the finite correlation length of quantum coherence. As an example, consider linear chains, i.e., conjugate polymers. Figure 6 systematically shows local coupling, nearest neighbor coupling, and next nearest neighbor coupling, etc. For a given set of parameters, the mapping to classical kinetics achieves convergence with increasing degree of nonlocality in kinetic coupling, which defines a measure of the spatial extent of exciton states in dissipative environments.

For the linear chain configuration, the rate expression in eq 17 depends on the absolute value of the coupling matrix element and is independent of the quantum phase. Coherent phase modulation does not exist in linear one-dimensional chain configurations but can play a significant role in nonlinear spatial arrangements with closed loops. In the presence of closed loops, different pathways along loops carry different phases and therefore lead to quantum phase interference. In the next section, we present explicit calculations of three-site and four-site systems arranged in the closed loop configuration.

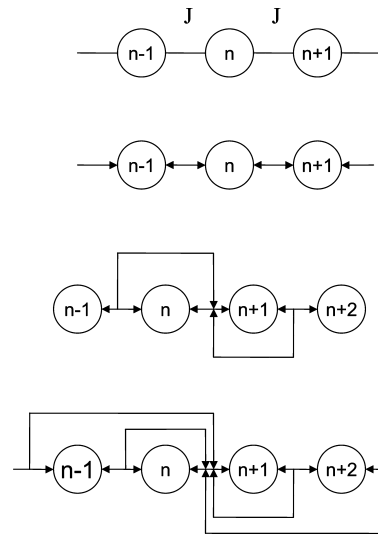

Figure 6. Mapping of an N-site exciton system in the linear configuration to a kinetic system of linear chain, with systematic incorporation of nonlocal kinetic couplings.

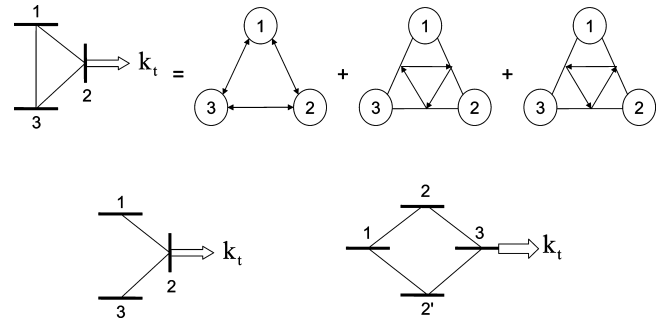

Figure 7. (a) Mapping of a three-site system in the closed loop configuration to three-state kinetics with quantum corrections represented by nonlocal links. (b) A three-site system in an open configuration. (c) A four-site system in a closed loop configuration.

V. Nonlinear Configuration: Pathway Interference

The discussion in the previous section is limited to linear molecular arrangements, which approximately represent molecular wires and other quasi one-dimensional systems. However, physical systems are rarely one-dimensional and are often topologically configured with multiple transfer pathways.[23,48] Even one-dimensional chains can form nonlinear topologies due to through-space couplings or interchain hoppings[49,50] Therefore, a particularly interesting mechanism is the interference between different transfer pathways, which is a quintessential quantum coherent effect. The simple three-site system in Figure 7 has two coupled exciton states and one trapping state and, therefore, exhibits modulation effects on the transfer rate as a dependence on the relative phase between the coupling matrix elements. Similar effects can be demonstrated in a three- or four-state model with bridge states[18] and in more realistic models.[51,52]

A. Three-Site System in the Closed Loop Configuration. For simplicity, we study the quantum phase modulation in a symmetric three-site system depicted in Figure 7. The exciton system contains a superexchange coupling through the bridge state and a direct coupling through space. The two coupling pathways may carry different phases, which modulate the average trapping time. The parameters for the model are taken as $J_{23} = J_{31} = J$, $\Delta_{12} = 0$, $\Delta_{23} = -\Delta_{31} = \Delta$, $\Gamma_{12}^* = \Gamma_{23}^* = \Gamma_{31}^* = \Gamma^*$, and $J_{12} = e^{i\theta}|J_{12}|$, where θ is the relative phase between the coupling matrix elements. The initial population is equally distributed between state 1 and 2, i.e., $\rho_1(0) = \rho_2(0) = {}^1/_2$. For the special case of real J_{12}, we solve the Bloch equation and obtain the average trapping time

$$\langle t \rangle = \frac{3}{k_t} + \frac{1}{\Gamma^*} + \frac{1}{2J^2}\frac{\Gamma^2 + (\Delta + J_{12})^2}{\Gamma} \qquad (22)$$

where $\Gamma = \Gamma^* + k_t/2$. The numerator in eq 22, $\Delta + J_{12}$, depends on the relative sign of the coupling matrix J_{12} and the detuning Δ, resulting in phase-sensitive interference. This phase effect introduces a difference in the average time due to the sign flip, $|\langle t \rangle_+ - \langle t \rangle_-| = 2(|\Delta J_{12}|)/(J^2\Gamma)$, which increases with detuning and decreases with dephasing rate. Equation 22 differs from the result for the two-site system in eq 4 because of a different coefficient for the average trapping rate k_t and a different numerator $\Delta + J_{12}$. To understand eq 22, we diagonalize the system Hamiltonian and obtain the eigenstates, i.e, excitons. One eigenstate has eigen energy of $\Delta + J_{12}$ and forms an effective two-state with the trap. The effective two-site system is responsible for the first and third terms in eq 22 and explains the interference effect due to the sign flip of J_{12}. Interestingly, the other eigenstate is orthogonal to the trap state, and relaxes only via pure dephasing, thus giving rise to $1/\Gamma^*$ in eq 22.

It is, however, misleading to use eq 22 to predict the optimal trapping time, because the expression is derived for real values of the coupling constant. To explore the complete parameter space including phase of J_{12}, we numerically solve the Bloch equation and plot $\langle t \rangle$ as a function of θ and Δ in Figure 8. The magnitude of exciton coupling J is taken as the basic energy unit, and other parameters are scaled as $\Gamma^* = J$, $|J_{12}| = J$, and $k_t = J$. Interesting, for small values of Δ, the minimal trapping time is located at $\theta = \pm \pi/2$ (the imaginary axis of J_{12}), whereas, for large values of Δ, the minimal trapping time is located at $\theta = 0$ or $\theta = \pi$ (the real axis of J_{12}). For large positive detuning ($\Delta > \Gamma$), the minimal trapping time is at $\theta = 0$, and the maximal trapping time is at $\theta = \pm\pi$; for large negative detuning ($\Delta <$

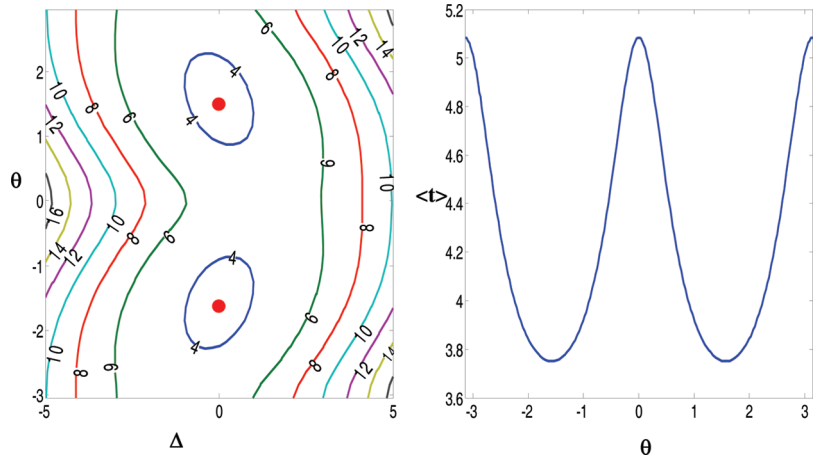

Figure 8. Average trapping time as a function of phase θ and Δ for the closed-loop three-state model with $|J| = J = 1$, $\Gamma^* = J$, and $k_t = J$ (the left contour plot) and the average trapping time as a function of phase θ for the same model with $\Delta = 0$ (the right plot).

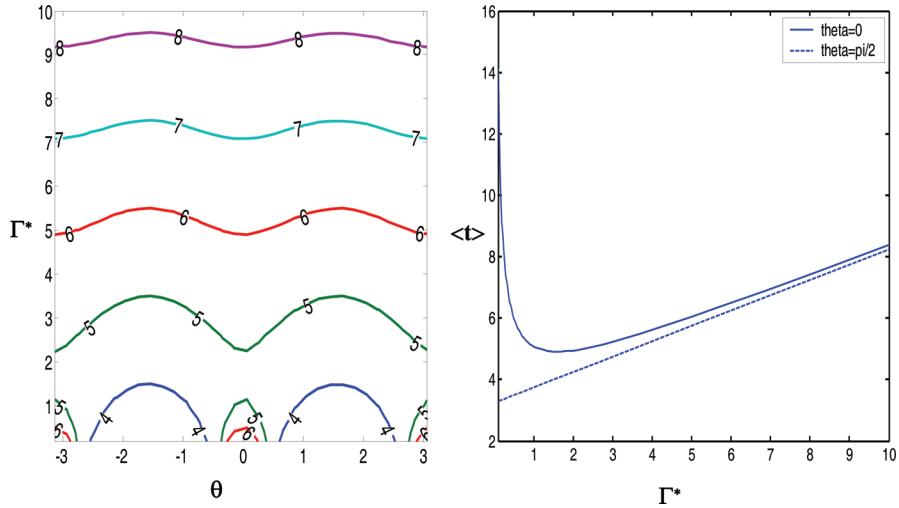

Figure 9. Average trapping time as a function of phase θ and Γ^* for the closed-loop three-state model with $|J| = J = 1$, $\Delta = 0$, and $k_t = J$ (the left contour plot) and the average trapping time as a function of dephasing rate Γ^* for the same model with $\theta = 0$ (solid curve) and $\theta = \pi/2$ (dash curve), respectively (the right plot).

$-\Gamma$), the maximal trapping time is at $\theta = 0$ and the minimal trapping time is at $\theta = \pm\pi$. Thus, for real values of J_{12}, the dependence of the trapping time as a function of Δ is consistent with the prediction in eq 22. Numerical search of parameter space identifies the minimal trapping time at $\Gamma^* = 0$, $k_t = 2(3J^2 + \Delta^2)^{1/2}$, and $\theta = \pm\pi/2$. The optimal value of k_t takes the same functional form as those derived for two-site, three-site, and linear chain systems in section III. As expected, the amplitude of phase modulation can be suppressed by dephasing. The dependence on the pure dephasing rate in Figure 9 confirms this prediction. Further, the average time has an optimal value as a function of Γ^* for $\theta = \pi/2$ but has a linear-dependence on Γ^* for $\theta = 0$, and the two curves converge at large dephasing rate.

B. Kinetic Mapping and General Interpretations. To interpret the finding of the global minimal at $\theta = \pm\pi/2$ predicted above, we apply the mapping procedure developed in section IV to the three-site system. Iterating eq 11 to leading order correction, we obtain the effective rate equation

$$\begin{aligned}\dot{\rho}_1 &= -(k_{12} + k_{12}^-)(\rho_1 - \rho_2) + (k_{31} - k_{31}^+) \times \\ &\qquad (\rho_3 - \rho_1) + (k_{23}^+ + k_{23}^-)(\rho_2 - \rho_3) \\ \dot{\rho}_2 &= -(k_{23} + k_{23}^-)(\rho_2 - \rho_3) + (k_{12} - k_{12}^+) \times \\ &\qquad (\rho_1 - \rho_2) + (k_{31}^+ + k_{31}^-)(\rho_3 - \rho_1) \\ \dot{\rho}_3 &= -(k_{31} + k_{31}^-)(\rho_3 - \rho_1) + (k_{23} - k_{23}^+) \times \\ &\qquad (\rho_2 - \rho_3) + (k_{12}^+ + k_{12}^-)(\rho_1 - \rho_2)\end{aligned} \tag{23}$$

As shown in Figure 7, we denote the clockwise nonlocal coupling (forward) with a positive sign, k^+, and counterclockwise nonlocal coupling (backward) with a negative sign, k^-. The classical rate constant k is defined by eq 14, and the high-order rate constants associated with nonlocal coupling are given by

$$\begin{aligned}k_{12}^+ &= 2\,\mathrm{Im}\,\frac{J_{13}J_{32}J_{21}}{\tilde{\Gamma}_{23}\tilde{\Gamma}_{21}} \\ k_{12}^- &= 2\,\mathrm{Im}\,\frac{J_{13}J_{32}J_{21}}{\tilde{\Gamma}_{31}\tilde{\Gamma}_{21}}\end{aligned} \tag{24}$$

and similarly for other k^- and k^+. For relatively small detuning ($\Delta < \Gamma^*$), the nonlocal rate constant for the three-site system is proportional to $\mathrm{Im}[J_{13}J_{32}J_{21}]$, the imaginary part of the product of the coupling matrix elements along the closed loop. Thus, phase modulation is characterized by the cumulative phase along the loop, $\theta_c = \theta_{13} + \theta_{32} + \theta_{21}$, and the optimal trapping time occurs at $\theta_c = \pm\pi/2$. For relatively large detuning, ($\Delta > \Gamma^*$), the magnitudes of the rate constants in eq 24 take the maximal value when J_{12} takes a real value, i.e., $\theta_c = 0$ and $\theta_c = \pi$. The leading order quantum correction correctly captures the main feature of the phase modulation in the three-site system. In addition, numerical solutions to eq 23 compare favorably with the exact result and become more accurate as the dephasing rate or the detuning increases.

We now generalize eq 24 to predict the phase modulation in a N-state loop and predict phase coherence in realistic exciton systems.

- Evidently, open topological structures without closed loops such as the dendrimers in Figure 13 will not display any phase modulation. Closed topological structures such as the light harvesting systems II in Figure 13 will exhibit phase modulation, similarly to the interference effect in the double slit experiment.
- To leading order, phase modulation is governed by the cumulative phase along a closed loop, $\theta_c = \theta_{12} + \theta_{23} + ... + \theta_{N,1}$. When the states along the loops are close to resonant or have a small offset $\Gamma^* > \Delta$, the extreme occurs on the real axis for an even number of links along the loop, $\theta_c = 0, \pm\pi$, and occurs on the imaginary axis for an odd number of links, $\theta_c = \pm\pi/2$.
- The situation is more complicated as the detuning increases. For large detuning $\Gamma^* < \Delta$, the phase-dependence is governed by the effective cumulative phase $\theta_c = \theta_{12} + \theta_{23} + ... + \theta_{N,1} + \theta_\Delta$, with θ_Δ as the additional contribution associated with the detuning along the loop.
- The phase-dependence becomes weaker as the dephasing rate or the trapping rate increases

C. Three-Site System in the Open Configuration. To illustrate the above predictions, we consider two additional examples. The first example is the open three-site system in Figure 7, where the link between states 1 and 2 is removed. For the symmetric three-site system, we define $\epsilon_1 = \epsilon_3 = \Delta$ and introduce a similar set of parameters as in eq 22 but with $J_{31} = 0$. Then, the expression for the average trapping time can be obtained similarly as in eq 6, giving

$$\begin{aligned}\langle t\rangle = \frac{3}{k_t} &+ \frac{1}{4|J_{12}|^2}\left[\Gamma_{12} + \frac{1}{\Gamma_{31}}[|J_{12}|^2 + |J_{23}|^2] + \right. \\ &\left.\frac{\Delta^2}{\mathrm{Det}}\left(\Gamma_{23} + 2\frac{|J_{12}|^2}{\Gamma_{31}}\right)\right] + \frac{1}{4|J_{23}|^2}\left[\Gamma_{23} + \frac{1}{\Gamma_{31}}[|J_{12}|^2 + |J_{23}|^2] + \right. \\ &\left.\frac{\Delta^2}{\mathrm{Det}}\left(\Gamma_{12} + 2\frac{|J_{23}|^2}{\Gamma_{13}}\right)\right]\end{aligned} \tag{25}$$

where $\Delta_{12} = -\Delta_{23} = \Delta$, $\Delta_{31} = 0$, $\Gamma_{31} = \Gamma_{31}^*$, $\Gamma_{12} = \Gamma_{12}^* + k_t/2$, $\Gamma_{23} = \Gamma_{23}^* + k_t/2$, and $\mathrm{Det} = \Gamma_{12}\Gamma_{23} + (|J_{23}|^2\Gamma_{23} + |J_{12}|^2\Gamma_{12})/\Gamma_{31}$. Under the special condition of identical coupling constants $J = |J_{12}| = |J_{23}|$ and identical dephasing rates $\Gamma^* = \Gamma_{12}^* = \Gamma_{23}^* = \Gamma_{31}^*$, eq 25 reduces to

$$\langle t\rangle = \frac{3}{k_t} + \frac{1}{\Gamma^*} + \frac{1}{2|J|^2}\frac{\Gamma^2 + \Delta^2}{\Gamma} \tag{26}$$

with $\Gamma = \Gamma^* + k_t/2$. In comparison with eq 22, eqs 25 and 26 depend only on the absolute value of the coupling constant $|J|$ and are therefore independent of the phase θ. The open configuration of the three-site system in Figure 7 is simply a variation of the linear chain configuration in Figure 3, and does not form a loop.

Interestingly, in this configuration, the optimal condition for eq 26 is a pair of nonvanishing rates, Γ^* and k_t, which differ from the optimal condition for eq 7. In Figure 10, the average trapping time $\langle t\rangle$ is plotted as a function of Γ^* and k_t for the open-loop model with $\Delta = J = 1.0$. From the contour, we can identify the optimal condition as $\Gamma^* = 1.4840$ and $k_t = 3.6349$, which defines the minimal value of $\langle t\rangle = 3.3014$. The vanishing optimal value of pure dephasing rate $\Gamma^* = 0$ in the linear chain configuration is an exception, and the general optimal condition for a complex network is defined by nonzero values of Γ^* and k_t.

D. Four-Site System in the Closed Loop Configuration. Our second example is the four-site system in Figure 7. Similar to the three-site system in the closed-loop configuration, the two

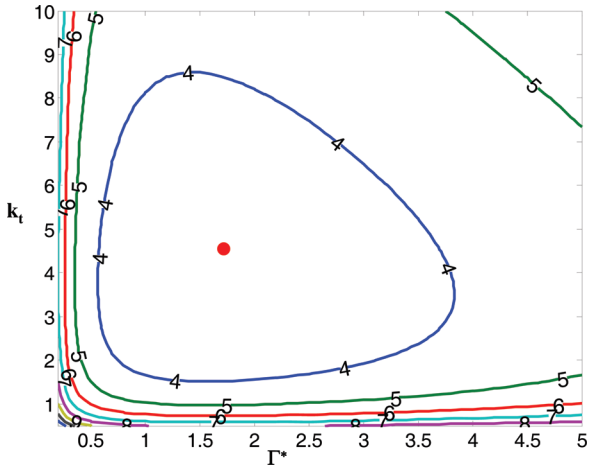

Figure 10. Contour plot of the average trapping time as a function of the trapping rate k_t and dephasing rate Γ^* for the open three-state model with $|J| = 1.0$ and $\Delta = 1.0$. The minimal trapping time is $\langle t \rangle = 3.3014$ with the optimal condition of $\Gamma^* = 1.484$ and $k_t = 3.6349$.

energy transfer pathways from the initial state 1 to the trap state 3 may carry different phases that lead to phase modulation as a result of quantum interference. The parameters for the four-site system are scaled with the absolute value of $J = |J|$, giving $\epsilon_2' = \epsilon_2 = \Delta$, $\epsilon_1 = \epsilon_4 = 0$, $\Gamma^* = J$, $k_t = J$, $J_{12'} = J_{2'3} = J_{23} = J$, and $J_{12} = Je^{i\theta}$. The average trapping time is plotted in Figure 11 as a function of detuning Δ and relative phase θ and then plot as a function of θ for a given value of $\Delta = 0$. As expected, the average trapping time $\langle t \rangle$ is modulated by θ, and the extreme value occurs on the real axis of the coupling constant, $\theta = 0, \pm\pi$. The difference between the four-site system and the three-site system (i.e., Figure 11 versus Figure 8) can be explained using kinetic mapping. Similarly to Figure 9, we calculate the dependence on the pure dephasing rate in Figure 12 and confirm the amplitude of phase modulation decreases as the dephasing rate Γ^* increases. Further, the average time has an optimal value as a function of Γ^* for $\theta = \pi$ but has a linear dependence on Γ^* for $\theta = 0$, and the two curves converge at large dephasing rate.

Spatial arrangements of molecular structures are ubiquitous in tabular systems, molecular wires, dendrimers, and polymeric liquid crystals. The spatial arrangements in these molecular structures exhibit subtle quantum effects if the quantum excitation is spatially extended or delocalized. For example, the open tree structure in dendrimers in Figure 13 will not display any phase modulation,[53] whereas the closed topological structure of the light harvesting systems II (LH2) in Figure 13 will exhibit phase modulation along every closed loop.[54] Multiple transfer pathways and their interference have been investigated in the context of long-range electron transfer in proteins[18,51,52,55] but can be better demonstrated in exciton systems[35] because energy excitation does not polarize the medium as strongly as charge excitation and hence is typically less localized than charge transfer systems.

VI. Concluding Remarks

The theoretical analysis presented in this paper consists of two related problems: optimization of exciton trapping efficiency and mapping of quantum energy transfer processes to network kinetics with nonlocal connectivity. Using these approaches, we can solve the minimal models to capture the underlying physics of efficient energy transfer and analyze these models thoroughly to quantify and classify the generic mechanisms.

For photosynthetic systems, the energy transfer efficiency approaches unity and is thus determined largely by the average trapping time, which reduces the problem to mean first passage time calculations and thus simplifies the analysis considerably. Analytical solutions for multisite systems show that environments can be optimized to yield minimal trapping time or maximal energy transfer efficiency, and the optimal conditions for the environments can be explained using the simple physical arguments:

1. The competition between coherent exciton dynamics and localized hopping or trapping yields the optimal value of trapping rate k_t for efficient energy transfer. The optimal value of k_t is a complex function of the exciton coupling J, detuning Δ, and dephasing rate Γ^*, and is generally nonzero.
2. Line-broadening increases the frequency overlap and therefore decreases the effective detuning, thus defining an optimal pure dephasing rate Γ^* for maximal efficiency. This effect does not play a role in a homogeneous linear chain with an identical site energy and with an end trap in Figure 3a, where pure dephasing does not assist quantum transfer. For an inhomogenous linear chain with an end trap as in Figure 3b, the optimal pure dephasing rate becomes nonzero in some regimes of the trapping rate but remains zero in the other regimes. Thus, dephasing assisted energy transfer is a complicated mechanism, which may or may not play a dominant role depending on the combined effect of the exciton coupling, detuning, and trapping.

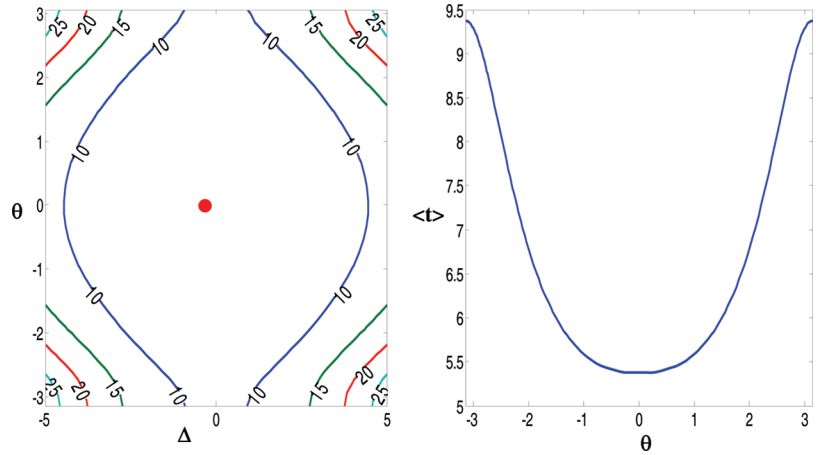

Figure 11. Average trapping time as a function of phase θ and Δ for the closed-loop four-state model with $|J| = J = 1$, $\Gamma^* = J$, and $k_t = J$ (the left contour plot) and the average trapping time as a function of phase θ for the same model with $\Delta = 0$ (the right plot).

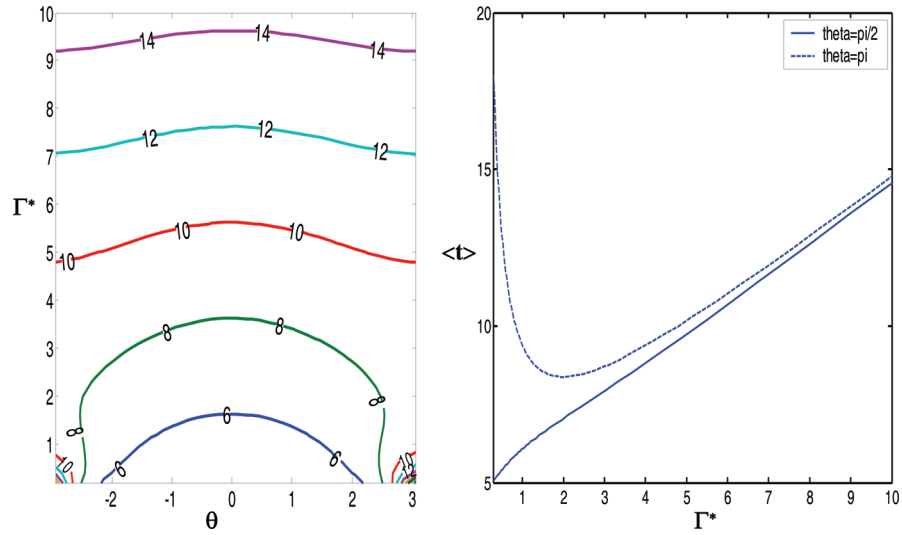

Figure 12. Average trapping time as a function of phase θ and Γ^* for the closed-loop four-state model with $|J| = J = 1$, $\Delta = 0$, and $k_t = J$ (the left contour plot) and the average trapping time as a function of phase Γ^* for the same model with $\theta = \pi/2$ (solid curve) and $\theta = \pi$ (dash curve), respectively (the right plot).

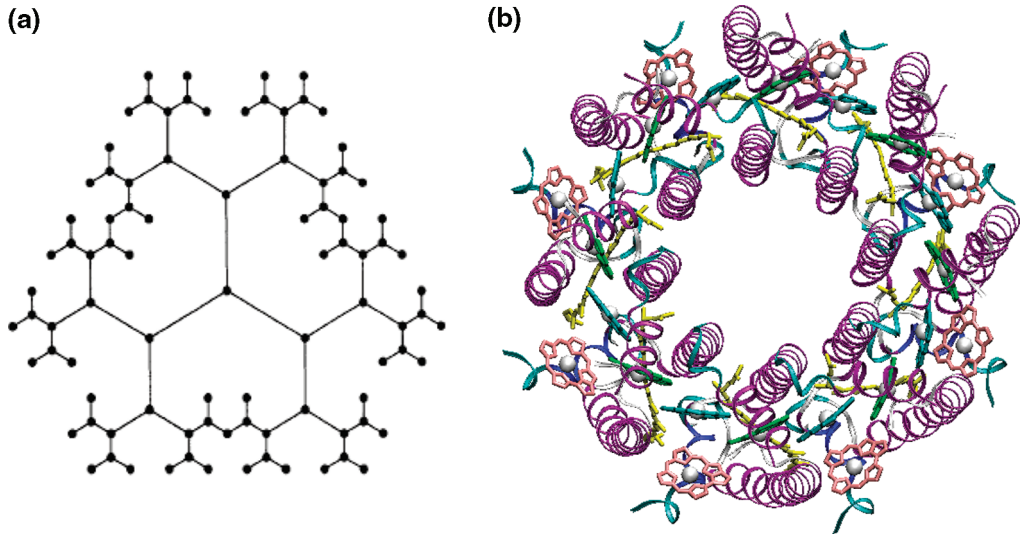

Figure 13. Examples of open and closed structures: (a) compact phenylacetylene dendrimers (reprinted with permission from *Chemical Physics*, copyright 2002 Elsevier: Chem. Phys. 2002, 275, 333.) and (b) LH2 Octameric complex from *Rs. Molishcianum*. This image is made with *VMD* (*J. Mol. Graphics* **1996**, *14*, 33−38) using a file owned by the Theoretical and Computational Biophysics Group, NIH Resource for Macromolecular Modeling and Bio-informatic, at the Beckman Institute, University of Illinois at Urbana-Champaign (*Structure* **1996**, *4*, 581).

3. Dephasing between two or more parallel pathways helps suppress destructive interference effects in nonlinear network configurations (i.e., energy transfer networks). Specifically, for an open loop configuration as in Figure 7b, the average trapping time is optimized at a nonzero pure dephasing rate but is phase-insensitive, whereas for a closed loop configuration in Figure 7a and in Figure 7c, the average trapping time is phase-sensitive. In contrast to linear configurations, the optimal dephasing rate for efficient trapping is typically nonzero in nonlinear network configurations.
4. Phase modulation of the trapping time arises from the interference between different energy transfer pathways and exists in energy transfer networks that form at least one closed loop. The cumulative phase along the loop determines the maximal and minimal trapping times, which occur when the product of the coupling matrix elements along the loop is an imaginary variable for an odd number of links as in Figure 7a and when the product is a real variable for an even number of links as in Figure 7c. To our knowledge, phase-sensitive modulation is a new observation that has not been analyzed before.

Though realistic exciton systems are more complicated, simple few-level systems discussed in this paper capture the essence of the optimal conditions. In fact, with simple variations of the three-state system in Figure 14, we are able to understand and classify all the optimal conditions discussed above: (1) The homogeneous linear chain in Figure 14a explains the optimal trapping time. (2) The biased linear chain in Figure 14b explains the optimal condition with nonzero optimal dephasing rate at large detuning. (3) The nonlinear two-branch system in Figure 14c explains the global optimal condition with combined trapping and dephasing time. (4) The nonlinear closed-loop system in Figure 14d explains the phase-modulation effects.

An energy transfer system can be mapped to a kinetic network with effective hopping rates as the leading order picture, which is then corrected by incorporating nonlocal links resulting from quantum mechanical corrections. The rate constants for the nonlocal links are phase insensitive when calculated along a

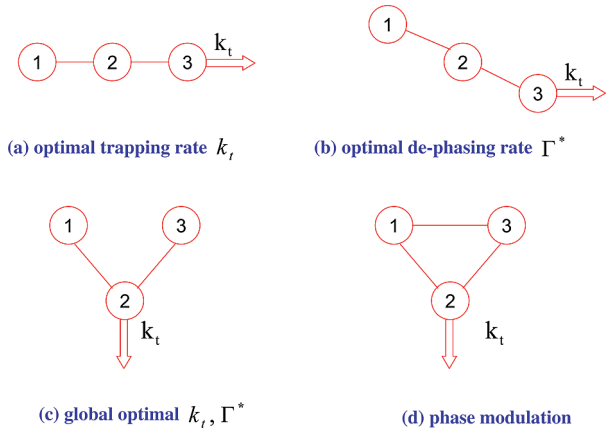

Figure 14. Variations of three-level system employed to classify the optimal conditions in more complex and realistic exciton systems: (a) homogeneous linear chain; (b) biased linear chain; (c) nonlinear two-branch system; (d) nonlinear closed-loop system.

chain segment and are phase sensitive when calculated along a closed loop. Thus, the mapping procedure systematically incorporates the classical hopping kinetics, phase-independent nonlocal quantum corrections, and phase-dependent nonlocal interference effects. As a result, this approach defines a rigorous and natural separation of classical hopping and quantum coherence, and introduces an intuitive tool to analyze topological connectivity and pathway interference in quantum networks.

Using the kinetic mapping procedure, we can estimate the quantum mechanical effects and show that the homogeneous linear chain configuration (see Figure 3) is mostly classical whereas the loop configuration requires significant quantum corrections. The two optimal conditions (1) and (2) discussed above for linear chains can be qualitatively predicted by classical kinetics, whereas the optimal conditions (3) and (4) for networks are due to nonlocal interference effects that cannot be predicted by classical hopping kinetics. When quantum mechanics is the dominant effect, the exciton basis representation of the same dynamic equation is more adequate than the local basis set used in classical hopping kinetics. In fact, the optimal conditions (3) and (4), specifically the topological dependence and phase modulation described in section V, can be better understood and estimated within the exciton basis representation and are therefore quantum mechanical in nature.

In summary, the results reported in this paper are derived for multisite systems in the local basis representation but can be instructive for mechanistic studies of natural photosynthetic systems and for the optimal design of artificial systems. The simple analytical solutions for the minimal models capture the essential physics involved in numerical simulations published earlier, predict a new observation of phase-sensitive interference in closed-loop configurations, and quantitatively classify different roles of environments in energy transfer processes. Furthermore, the kinetic mapping approach applies to quantum transport in general, especially for charge transfer processes such as electron transfer in biological systems, electric current in molecular electronics, and carrier mobility in molecular crystals or conjugate polymers.[15,55,56]

Acknowledgment. The work described here is supported by the National Science Foundation (0806266 and 0556268) and MIT energy initiative seed grant (MITEI). We thank Mr. Fan Liu and Dr. Jianlan Wu for preparing some of the figures. We also thank the reviewers for bringing us to the attention of several recent references, which are discussed in the introduction. The calculations reported in this paper were completed in the summer of 2008 and a draft was circulated thereafter.

References and Notes

(1) Sauer, K. Photosynthesis--the light reactions. *Annu. Rev. Phys. Chem.* **1979**, *30*, 155.

(2) Blankenship, R. E. *Molecular Mechanisms of photosynthesis*; Blackwell Science: Oxford/Malden, 2002.

(3) van Grondelle, R.; Novoderezhkin., V. I. Energy transfer in photosynthetic experimental insights and quantitative models. *Phys. Chem. Chem. Phys.* **2006**, *8*, 793.

(4) Engel, G. S.; Calhoun, T. R.; Read, E. L.; Ahn, T.; Mancal, T.; Cheng, Y. C.; Blankenship, R. E.; Fleming, G. R. Evidence for wavelike energy transfer through quantum coherence in photosynthetic systems. *Nature* **2007**, *446*, 782 Letters.

(5) Lee, H.; Cheng, Y. C.; Fleming, G. R. Coherence dynamics in photosynthesis: Protein protection of excitonic coherence. *Science* **2007**, *316*, 1462.

(6) Gust, D.; Moore, T. A.; Moore, A. L. Mimicking photosynthetic solar energy transduction. *Acc. Chem. Res.* , *26*, 198–205.

(7) Leegwater, J. A.; Durrant, J. R.; King, D. R. Exciton equilibrium induced by phonons: Theory and application to ps ii reaction centers. *J. Chem. Phys.* **1997**, *101*, 7205.

(8) Vulto, S. I. E.; de Baat, M. A.; Louwe, R. J. W.; Permentier, P.; Neef, T.; Miller, M.; van Amerongen, H.; Aartsma., T. J. Exciton simulations of optical spectra of the fmo complex from the green sulfur bacterium chlorobium tepidum at 6k. *J. Phys. Chem. B* **1998**, *102*, 9577.

(9) Tretiak, S.; Middleton, C.; Chernyak, V.; Mukamel, S. Bacteriochlorophyll and carotenoid excitonic coupings in the lh2 system of purple bacteria. *J. Phys. Chem. B* **2000**, *104*, 9540.

(10) Abramavicius, D.; Palmieri, B.; Voronine, D. V.; Sanda, F.; Mukamel, S. Coherent multidimensional optimal spectroscopy. *Chem. Rev.* **2009**, *109*, 2350.

(11) Sener, M. K.; Lu, D.; Ritz, T.; Park, S.; Fromme, P.; Schulten, K. Robustness and optimality of light harvesting in cyanobacterial photosystem i. *J. Phys. Chem. B* **2002**, *106*, 7948.

(12) Sener, M. K.; Park, S.; Lu, D.; Damjanovic, A.; Ritz, T.; Fromme, P.; Schulten, K. Excitation migration in trimeric cyanobacterial photosystem i. *J. Chem. Phys.* **2004**, *120*, 11183.

(13) Cho, M.; Vaswani, H. M.; Brixner, T.; Stenger, J.; Fleming, G. R. Exciton analysis in 2d electronic spectroscopy. *J. Phys. Chem.* **2005**, *109*, 10542.

(14) Adolphs, J.; Renger, T. How proteins trigger excitation energy transfer in the fmo complex of green sulfur bacteria. *Biophys. J.* **2006**, *91*, 2778.

(15) Silbey, R. J. Electronic energy transfer in molecular crystals. *Annu. Rev. Phys. Chem.* **1976**, *27*, 203.

(16) Cheng, Y. C.; Silbey, R. J. Coherence in the b800 ring of purple bacteria lh2. *Phys. Rev. Lett.* **2006**, *96*, 028103.

(17) Jang, S.; Newton, M. D.; Silbey, R. J. Multichromophoric forster resonance energy transfer from b800 to b850 in the light harvesting complex 2: Evidence for subtle energetic optimization by purple bacteria. *J. Phys. Chem. B* **2007**, *111*, 6807.

(18) Jang, S.; Cao, J. Non-adiabatic instanton calculation of multi-state electron transfer reaction rate: interference effects in three and four state systems. *J. Chem. Phys.* **2001**, *114*, 9959.

(19) Denschlag, J.; Simsarian, J. E.; Feder, D. L.; Clark, C. W.; Collins, L. A.; Cubizolles, J.; Deng, L.; Hagley, E. W.; Helmerson, K.; Reinhard, W. P.; Rolston, S. L.; Schneider, B. I.; Phillips, W. D. Generating solitons by phase engineering of a bose-einstein condensates. *Science* **2000**, *287*, 97.

(20) Kral, P.; Shapiro, M. Cyclic population transfer in quantum systems with broken symmetry. *Phys. Rev. Lett.* **2001**, *87*, 183002.

(21) Li, X.; Wu, Y.; Steel, D.; Gammon, D.; Stivater, T. H.; Katzer, D. S.; Park, D.; Piermarocchi, C.; Sham, L. J. An all-optical quantum gate in a semiconductor quantum dot. *Science* **2003**, *301*, 809.

(22) Franco, I.; Shapiro, M.; Brumer, P. Robust ultra-fast currents in molecular wires through start shifts. *Phys. Rev. Lett.* **2007**, *99*, 126802.

(23) Didraga, C.; Knoester, J. Excitons in tabular molecular aggregates. *J. Lumin.* **2004**, *110*, 239.

(24) Heijs, D.; Malyshev, V. A.; Knoester, J. Trapping time statistics and efficiency of transport of optical excitations in dendrimers. *J. Chem. Phys.* **2004**, *121*, 4884.

(25) Reineker, P.; Engelmann, A.; Yudson, V. I. Excitons in dendrimers: optical absorption and energy transport. *J. Lumin.* **2001**, *94−95*, 203.

(26) Reineker, P.; Engelmann, A.; Yudson, V. I. Optical absorption and energy transfer processes in dendrimers. *J. Lumin.* **2004**, *108*, 333.

(27) Hemenger, R. P.; Pearlstein, R. M. Impurity quenching of molecular excitons ii. frenkel excitons in linear chains. *Chem. Phys.* **1973**, *2*, 424.

(28) Vlaming, S. M.; Malyshev, V. A.; Knoester, J. Nonmonotonic energy harvesting efficiency in biased exciton chains. *J. Chem. Phys.* **2007**, *127*, 154719-1.

(29) Gaab, K.; Bardeen, C. The effects of connectivity, coherence, and trapping on energy transfer in simple light-harvesting systems studied using the haken-strobl model with diagonal disorder. *J. Chem. Phys.* **2004**, *121*, 7813.

(30) Plenio, M. B.; Huelga, S. F. Dephasing-assisted transport: quantum networks and biomolecules. *New J. Phys.* **2008**, *10*, 113019.

(31) Caruso, F.; Chin, A. W.; Datta, A.; Huelga, S. F.; Plenio, M. B. Fundamental mechanisms of noise supported energy transfer in biological systems. *Quant. Phys.* 2009. arXiv:0901.445v1.

(32) Mohseni, M.; Rebentrost, P.; Lloyd, S.; Aspuru-Guzik, A. Environment-assisted quantum walks in energy transfer of photosynthetic complexes. *J. Chem. Phys.* **2008**, *129*, 174106.

(33) Rebentrost, R.; Mohseni, M.; Kassal, I.; Lloyd, S.; Aspuru-Guzik, A. Environment-assisted quantum transport. *New J. Phys.* **2009**, *11*, 033003.

(34) Liu, F. Cao, and J. Silbey. R. J. Manuscript in preparation.

(35) Olaya-castro, A.; Lee, C. F.; Olsen, F. F.; Johnson, N. F. Efficiency of energy transfer in a light-harvesting system under quantum coherence. *Phys. Rev., B* **2008**, *78*, 065115.

(36) Tannor, D. J.; Rice, S. A. Coherent pulse sequence control of product formation in chemical reactions. *Adv. Chem. Phys.* **1988**, *70*, 441–524.

(37) Brumer, P.; Shapiro, M. Coherence chemistry: controlling chemical reactions. *Acc. Chem. Res.* **1989**, *22*, 407.

(38) Peirce, A.; Dahleh, M.; Rabitz, H. Optimal control of quantum mechanical systems: Existence, numerical approximations, and application. *Phys. Rev. A* **1988**, *37*, 4950.

(39) Zhao, M.; Rice, S. *Optical control of molecular dynamics*; Wiley Inter-science: New York, 2000.

(40) Shapiro, M.; Brumer, P. *Principles of the Quantum Control of Atomic and Molecular Processes*; Wiley: New York, 2003.

(41) Cao, J.; Bardeen, C. J.; Wilson, K. R. Molecular p pulse for total inversion of electronic state population. *Phys. Rev. Lett.* **1998**, *80*, 1406.

(42) Chakrabarti, R.; Rabitz, H. Quantum control landscapes. *Int. Rev. Phys. Chem.* **2007**, *26*, 671–725.

(43) Silbey, R.; Harris, R. A. Variational calculation of the dynamics of a two level system interacting with a bath. *J. Chem. Phys.* **1984**, *80*, 2615.

(44) Tanimura, Y. Stochastic liouville, langevin, fokker-planck and master equation approaches to quantum dissipative systems. *J. Phys. Soc. Jpn.* **2006**, *75*, 082001.

(45) Cao, J. A phase-space study of bloch-redfield theory. *J. Chem. Phys.* **1997**, *107*, 3204.

(46) Cao, J.; Silbey, R. J. Generic schemes for single molecule kinetics: Self-consistent pathway solutions. *J. Phys. Chem.* **2008**, *112*, 12867.

(47) Hofmann, C.; Aartsma, T. J.; Michel, H.; Kohler, J. Direct observation of tiers in the energy landscape of a chromoprotein: A single-molecule study. *Proc. Natl. Acad. Sci. U.S.A.* **2003**, *100*, 15534.

(48) Vlaming, S. M.; Heijs, D. J.; Knoester, J. Transport of optical excitations on dendrimers in the continuum approximation. *J. Lumin.* **2005**, *111*, 349.

(49) Collini, E.; Scholes, G. D. Coherent inter-chain energy migration in a conjugated polymer at room temperature. *Science* **2009**, *323*, 369.

(50) Scholes, G. D.; Ghiggino, K. P.; Oliver, A. M.; Paddon-Row, M. N. Through-space and through-bond effects on exciton interactions in rigidly linked dinaphthyl molecules. *J. Am. Chem. Soc.* **1993**, *115*, 4345.

(51) Skourtis, S. S.; Waldeck, D. H.; Beratan, D. N. Inelastic electron tunneling erases coupling-pathway interferences. *J. Chem. Phys. B* **2004**, *108*, 15511.

(52) Prytkova, T. R.; Kurnikov, I. V.; Beratan, D. N. Coupling coherence distinguishes structure sensitivity in protein electron transfer. *Science* **2007**, *315*, 622.

(53) Nantalaksakul, A.; Reddy, D. R.; Bardeen, C. J.; Thayumanavan, S. Light harvesting dendrimers. *Photosynthesis Res.* **2006**, *87*, 133–150.

(54) McDermontt, G.; Prince, S. M.; Freer, A. A.; Hawthornthwaite, A. M.; Papiz, M. Z.; Cogdell, R. J.; Issacs, N. W. Crystal structure of an integral membrane light-harvesting complex from photosynthetic bacteria. *Nature* **1995**, *374*, 517.

(55) Beratan, D. N.; Onuchic, N.; Winkler, J.; Gray, H. B. Electron-tunneling pathways in proteins. *Science* **1992**, *258*, 1740.

(56) Mujica, V.; Kemp, M.; Ratner, M. A. Electron conduction in molecular wires. *J. Chem. Phys.* **1994**, *101*, 6849.

JP9032589